B. TECH. PROJECT REPORT

On

High Dynamic Range Imaging of Diffuse Emission in Galaxy Clusters

BY

Snigdh Mohan Singh

(130003035)

DISCIPLINE OF MECHANICAL ENGINEERING

INDIAN INSTITUTE OF TECHNOLOGY INDORE

High Dynamic Range Imaging of Diffuse Emission in Galaxy Clusters

A PROJECT REPORT

Submitted in partial fulfillment of the
requirements for the award of the degrees

of
BACHELOR OF TECHNOLOGY
in

MECHANICAL ENGINEERING

Submitted by:
Snigdh Mohan Singh

Guided by:
1) Dr. Abhirup Datta- Assistant Professor, Centre of Astronomy
2) Dr. Siddharth Malu- Associate Professor, Centre of Astronomy

INDIAN INSTITUTE OF TECHNOLOGY INDORE
December 2016

CANDIDATE'S DECLARATION

I hereby declare that the project entitled **"High dynamic Range Imaging of diffuse Emission in Galaxy Clusters"** submitted in partial fulfillment for the award of the degree of Bachelor of Technology in 'Mechanical' completed under the supervision of **Dr. Abhirup Datta [Assistant Professor, Centre of Astronomy] & Dr. Siddharth Malu [Assistant Professor, Centre of Astronomy],** IIT Indore is an authentic work.

Further, I declare that I have not submitted this work for the award of any other degree elsewhere.

Signature and name of the student(s) with date

CERTIFICATE by BTP Guide(s)

It is certified that the above statement made by the student is correct to the best of our knowledge.

Signature of BTP Guide(s) with dates and their designation

Preface

This report on "High Dynamic Range Imaging of Diffuse Emission in Galaxy Clusters" is prepared under the guidance of Dr. Abhirup Datta & Dr. Siddharth Malu.

Through this report I have tried to describe the processes involved in observations of diffuse emission in Galaxy clusters. The Cluster data is acquired from GMRT Pune and after data processing a calibrated Radio Image is generated.

I have tried to the best of my abilities and knowledge to explain the content in a lucid manner. I have also added plots and figures to make it more illustrative.

Snigdh Mohan Singh
B.Tech. IV Year
Discipline of Mechanical
IIT Indore

Acknowledgements

I wish to thank Dr. Abhirup Datta & Dr. Siddharth Malu for their kind support and valuable guidance. It is their help and support, due to which I was able to complete the design and technical report.

Without their support this report would not have been possible.

Snigdh Mohan Singh

B.Tech. IV Year

Discipline of Mechanical

IIT Indore

Abstract

Diffuse Radio Emissions are discovered in many galaxy clusters which intimates recent merging. Galaxy-cluster merger shocks efficiently accelerate the ambient electrons through diffusive shock acceleration and amplify magnetic field by compressing the Inter Cluster Medium. As a result, such objects produce a significant amount of synchrotron radio emission. Radio halo and Mpc scale peripheral radio relics thus help us to trace back the cluster formation history.

The focus of this work is to obtain the GMRT deep radio maps of diffuse emission from the massive clusters. We want to understand the effect of mergers on production of non-thermal emission. Here, we study the galaxy cluster MACSJ0417.5-1154. This cluster, at a redshift of 0.443, is one of the most X-ray luminous galaxy cluster in the MAssive Cluster Survey (MACS) with an X-ray luminosity in the 0.1–2.4 keV band of $2.9\times10\ 45$ erg s -1 .

The galaxy cluster MACSJ0417.5-1154 has been observed for nearly 9 hours in L-Band with Giant Metrewave Radio Telescope (GMRT). The bandwidth in which data was inspected is 33.33MHz with the central frequency of 1.38MHz. Data were processed using the Common Astronomy Software Application(CASA). RFI obliteration was carried out using the in-built flagdata tool in CASA. Algorithms such as TFcrop & RFlag were put into use to deal with RFI. After mitigating RFI effects, Calibration, imaging and self-calibration were carried out.

Table of Contents

List of Figures

Introduction

Radio Astronomy- Radio astronomy is the study of radio waves originating outside the Earth. The radio range of frequencies (ν) or wavelengths(λ) is loosely defined by three factors: atmospheric transparency, current technology, and fundamental limitations imposed by quantum noise. Together they yield a boundary between radio and far-infrared astronomy at frequency ν ~1 THz or wavelength λ= 0.3mm.

The radio window in uniquely broad, spanning roughly five decades of frequency (10 MHz to 1 THz) and wavelength. This has both scientific and practical consequences:

- A wide variety of astronomical sources, thermal and non-thermal radiation mechanisms, and propagation phenomena can be studied at radio wavelengths.
- A wide variety of radio telescopes and observing techniques are needed to cover the radio spectrum effectively.

The radio window was opened before observations in other wavebands could be made from above the atmosphere, so early radio astronomy was a science of discovery and serendipity. It revealed a "parallel universe" of unexpected sources never seen, or at least not recognized, by optical astronomers. Major discoveries of radio astronomy include:

- Non-thermal radiation from our Galaxy and other astronomical sources
- The violent universe of radio galaxies and quasars powered by supermassive black holes
- Cosmological evolution of galaxies and quasars
- Emission from cold interstellar gas
- Cosmic microwave background radiation from the big bang
- Neutron stars
- Gravitational radiation
- Extrasolar planets
- Gravitational lensing

With the advent of astronomy from space, the entire electromagnetic spectrum has become accessible. Many sources discovered by radio astronomers can be now studied in other wavebands, and new objects discovered in other wavebands (e.g., gamma-ray bursters) can be studied by radio astronomers. Radio astronomy is no longer a separate field; it is one facet of multi-wavelength astronomy.

Telescopes having very large diameters D are required for good angular resolution $\theta = \lambda/D$ radians at radio wavelengths. On the other hand, huge interferometers spanning D~ 10^4 km are practical and precision telescopes (e.g., having reflectors with rms surface errors $\sigma < \lambda/16$) can be built. Paradoxically, the finest angular resolution is obtainable at the long-wavelength (radio) end of the electromagnetic spectrum. Coherent (phase preserving) amplifiers are required for accurate interferometric imaging of faint extended sources because they allow the signal from each telescope in a multi-element interferometer to be amplified before combination with the signals from the other telescopes, rather than being divided among the other telescopes before combination. Aperture-synthesis interferometry at radio wavelengths provides unparalleled sensitivity, fidelity, resolution, and position accuracy. This is a huge practical advantage of radio astronomy.

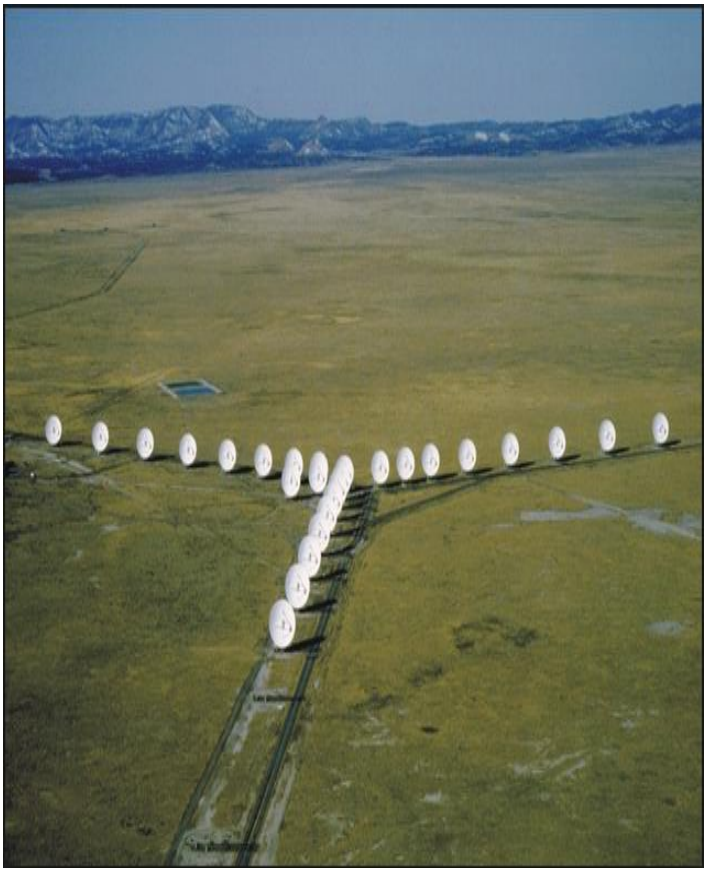

Figure 1: Very Large Array

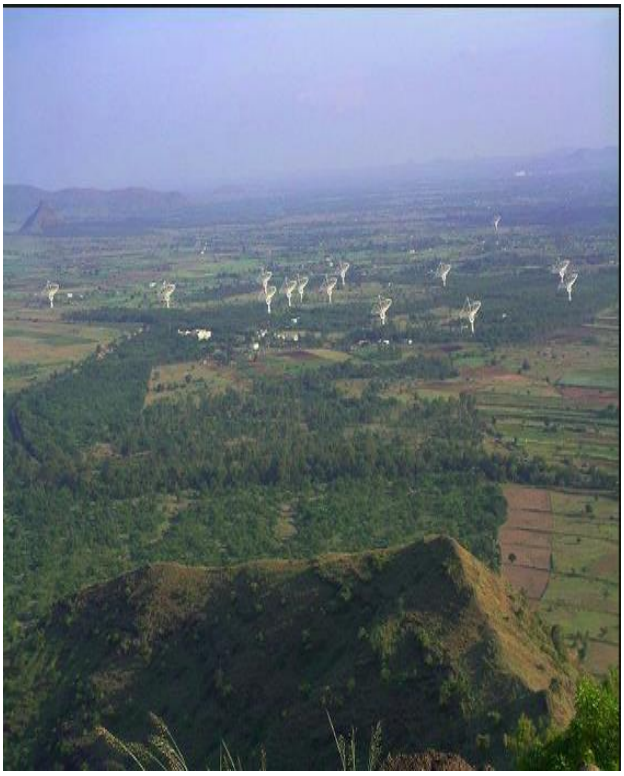

Figure 2: GMRT array

Galaxy Clusters- Galaxies love to cluster together. Their mutual gravity can draw galaxies together into a cluster that is several millions of light years across. Some clusters have only a handful of galaxies and are called poor clusters. Other clusters with hundreds to thousands of galaxies are called rich clusters. The low mass of a poor cluster prevents the cluster from holding onto its members tightly. The poor cluster tends to be a bit more irregular in shape than a rich cluster. Our Milky Way is part of a poor cluster called the **Local Group**.The Local Group has two large spirals, one small spiral, two ellipticals, at least 19 irregulars, at least 17 dwarf ellipticals and at least 5 dwarf spheroidals.The proportions of the different types of galaxies in the Local Group probably represents the number of the different types of galaxies in the rest of the universe. Clusters of galaxies formed late in the history of the Universe; in fact it appears some clusters are still growing through mergers. The hot, X-ray emitting, intergalactic medium trapped in the gravitational potential well of clusters is strongly affected by mergers. Strong shocks, rapid rotation, and turbulence are produced in the gas, all of which can be investigated through numerical simulation. The Galaxy Cluster that is used in this project is one of the objects studied in MAssive Cluster Survey(MACS) and is named **MASCSJ0417.5-1154** . This cluster, at a redshift of 0.443, is one of the most X-ray luminous galaxy cluster in the MACS.

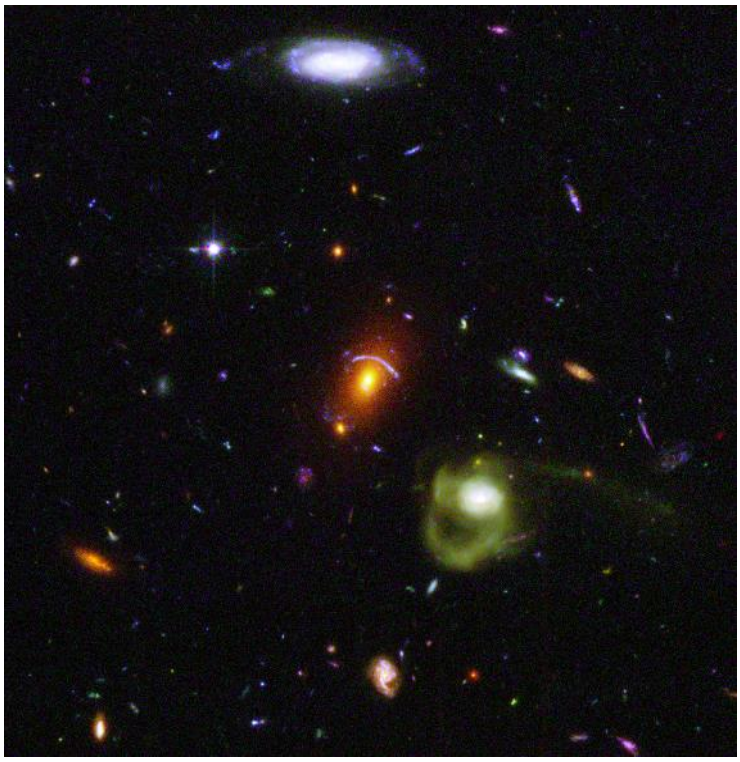

Figure 3: Deep Field Galaxies

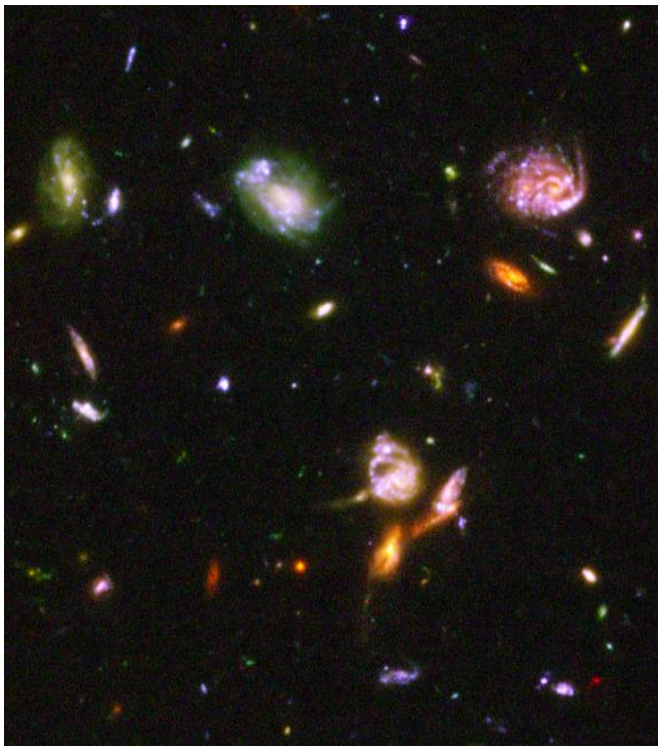

Figure 4: Figure 3: Deep Field Galaxies

Diffuse Emission- Galaxy-cluster merger shocks efficiently accelerate the ambient electrons through diffusive shock acceleration and amplify magnetic field by compressing the Inter Cluster Medium. As a result, such objects produce a significant amount of synchrotron radio emission. Radio halo and Mpc scale peripheral radio relics thus help us to trace back the cluster formation history. It is the merger hypothesis that provides the most plausible explanation for the presence of diffuse sources. The physical size of diffuse sources (> 0.5 Mpc) relative to their short lifetimes may be explained as a result of the reacceleration of electrons which are already dispersed over a large region. Cluster mergers, which can have collisional kinetic energy of ~10^57 J, are a likely source of the energy required to create and power diffuse sources.
Research in this field has been limited primarily by the difficulty of observing diffuse, low surface brightness sources. The field has evolved by looking for patterns and trends that may have a common physical origin. Trying to model how diffuse sources are created and sustained is even more challenging. A general problem of any astrophysics research is that one cannot observe the time development of most sources, as we only see them at a snapshot in time. For many types of sources, such as spiral galaxies, this is partially compensated for by the large numbers accessible to observation, each at different stages in their evolution. From these observations, a picture of the time evolution of the galaxies can be developed. Clearly that is not the case in this field, and any sense of time development must be obtained from estimates of the lifetime of the diffuse sources, and the characteristics of the phenomena that might cause them. Hence, the models are based on empirical evidence from what is still a relatively small sample.

GMRT - DATA for Galaxy Cluster **MASCSJ0417.5-1154** at 1.3GHz, one of the objects studied in MAssive Cluster Survey(MACS) is acquired from Giant Metrewave Radio Telescope (GMRT), located at a site about 80 km north of Pune, India. GMRT consists of 30 fully steerable gigantic parabolic dishes of 45m diameter each spread over distances of up to 25 km. The correlation of radio signals from all the 435 possible pairs of antennas or interferometers over several hours thus enable radio images of celestial objects to be synthesized with a resolution equivalent to that obtainable with a single gigantic dish 25 kilometre in diameter.

CASA- The Common Astronomy Software Applications infrastructure consists of a set of C++ tools bundled together under an iPython interface as a set of data reduction tasks. This structure provides flexibility to process the data via task interface or as a python script. Processing of data of **MASCSJ0417.5-1154** was accomplished using CASA.

Interferometry- The largest fully steerable dishes have diameters D~100 m. The angular resolution of a diffraction-limited telescope is $\theta = \lambda/D$ radians, so impossibly large diameters are needed to achieve sub-arcsecond resolution at radio wavelengths. Tracking accuracy is also a problem for a large single dish. The telescope beam should be able follow a radio source on the sky within $\sigma \sim \theta/10$ for reasonably accurate photometry or imaging. The accuracy with which the actual beam direction during an observation can be recovered by data analysis determines the accuracy with which the sky position of a radio source can be measured. Gravitational sagging, deformations caused by differential solar heating, and torques caused by wind gusts combine to limit the mechanical tracking and pointing accuracies. Interferometers comprising N>=2 moderately small dishes have mitigated these many other practical problems associated with single dishes, such as vulnerability to fluctuations in atmospheric emission and receiver gain, radio-frequency interference, and pointing shifts caused by atmospheric refraction.

The basic **interferometer** is a pair of radio telescopes whose voltage outputs are correlated (multiplied and averaged). Even the most elaborate interferometers with N>>2 elements can be treated as $N(N-1)/2$ independent interferometer pairs.

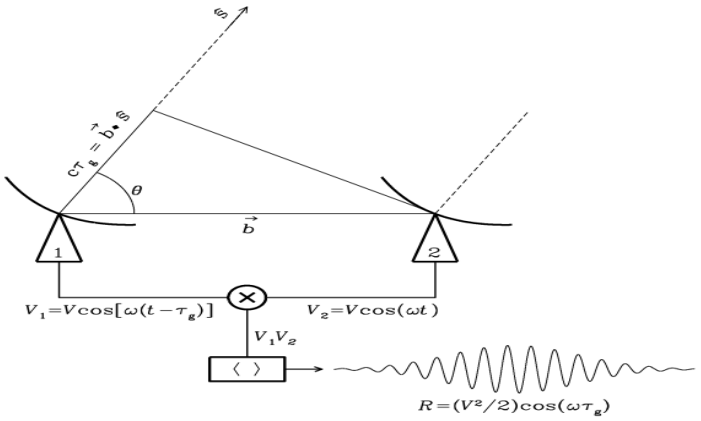

Figure 5: Two element interferometer

This block diagram shows the components of the simplest **two-element interferometer** observing in a very narrow frequency range centered on $\nu = \omega/2\pi$. The correlator multiplies and averages the voltage outputs V1 and V2 of the two dishes. **s** is the unit vector in the direction of a distant point source and **b** is the vector baseline from antenna 1 to antenna 2. The output voltage V1 of antenna 1 is the same as the output voltage V2 of antenna 2, but it is retarded by the geometric delay $\boldsymbol{\tau = b.s/c}$. These voltages are multiplied and time averaged by the correlator to yield an output response whose amplitude R is proportional to the point-source flux density and whose phase depends on the delay and the frequency. The quasi-sinusoidal output fringe shown occurs if the source direction in the interferometer frame is changing at a constant rate $d\theta/dt$. The broad Gaussian envelope of the fringe is caused by primary-beam attenuation if the individual dishes do not track the source.

Visibility- A fundamental property of the radio waves emitted by cosmic sources is that they are stochastic in nature, i.e. the electric field at Earth due to a distant cosmic source can be treated as a random process. A commonly used statistic for random processes is the auto-correlation function. The auto-correlation function is defined as

$$R(t,\boldsymbol{\tau})=\langle x(t)x(t+\boldsymbol{\tau})\rangle \ ,$$

where the angular brackets indicate taking the mean value.

The Fourier transform S(ν) of the auto-correlation function is called the power spectrum. A process whose auto-correlation function is a delta function has a power spectrum that is flat - such a process is called ``white noise". Many radio astronomical signals have spectra that are relatively flat; these signals can hence be approximated as white noise. Radio astronomical receivers however have limited bandwidths, that means that even if the signal input to the receiver is white noise, the signal after passing through the receiver has power only in a finite frequency range. Its auto-correlation function is hence no longer a delta function, but is a sinc function with a width ~1/Δν, where Δν is the bandwidth of the receiver. The bandwidth Δν is typically much smaller than the central frequency ν at which the radio receiver operates.

The signal received from a distant cosmic source is in general a function both of the receivers location as well as of time. Much as we defined temporal correlation functions above, one can also define spatial correlation functions. If the signal at the observer's plane at any instant is E(**r**), then spatial correlation function is defined as:

$$V(x)=\langle E(r)E(r+x)\rangle, \quad \text{In practice one averages over time}$$

The function V is referred to as the "**visibility function**" (or just the "**visibility**").

An interferometer measures the interference pattern observed by pairs of apertures. The interference pattern is directly related to the source brightness. In particular, for small fields of view the complex visibility, V(u,v), is the 2D Fourier transform of the brightness on the sky, T(x,y)

Fourier space/domain

$$V(u,v) = \int\int T(x,y)e^{2\pi i(ux+vy)}dxdy$$

$$T(x,y) = \int\int V(u,v)e^{-2\pi i(ux+vy)}dudv$$

Image space/domain

Visibility is a complex quantity expressed as (amplitude, phase). Single visibility V(u,v) contains information from the whole image I(l,m)– not just some part of it. Get a lot of visibilities in the (u,v) plane and construct the image.

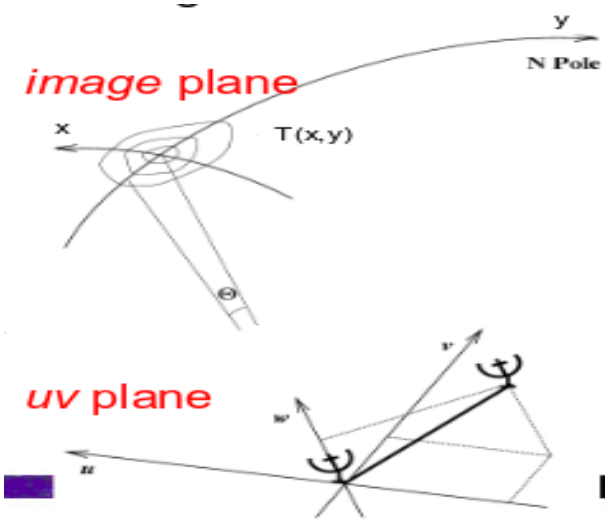

Figure 6: Image and Fourier Plane

Radio Frequency Interference

The radio signals arriving on Earth from astronomical objects are extremely weak -- millions (or billions) of times weaker than the signals used by communication systems. For example, a cellular telephone located on the Moon would produce a signal on Earth that radio astronomers consider quite strong. Because the cosmic radio sources are so weak, they are easily masked by man-made interference. Possibly even worse than complete masking, weaker interfering signals can contaminate the data collected by radio telescopes potentially leading astronomers to erroneous interpretations. By international agreement, radio frequencies are divided up into blocks, or bands, designated for different types of uses. For example, you know that AM radio stations all are within a certain range of frequencies that is different from the band of frequencies in which you find FM stations. Similarly, TV stations use different frequencies than, say, police two-way radios. These international frequency designations are designed to prevent one type of station from interfering with stations of another type.

A number of frequency bands are allocated to radio astronomy. Because radio astronomers do their work with extremely sensitive receiving equipment, *transmitting* is generally prohibited in the radio astronomy bands. However, transmitters using frequencies near those assigned to radio astronomy can cause interference to radio telescopes. This occurs when the transmitter's output is unduly "broad," spilling over into the radio astronomy frequencies, or when the transmitter emits frequencies outside its intended range. Other interference arises because radio transmitters often unintentionally emit signals at multiples of their intended frequency. As use of radio for devices such as cellular telephones, wireless computer networks, garage door openers, and a whole host of other uses continues to increase, the threats to radio astronomy from inadequately engineered transmitters increases. A prime threat comes from transmitters in orbiting Earth satellites, since those transmitters are located overhead, precisely where radio astronomers must aim their telescopes to study the Universe. In addition, many types of equipment not normally considered to be radio transmitters, particularly computers or systems incorporating microprocessors, emit undesirable radio signals.

Identifying RFI in GMRT data-

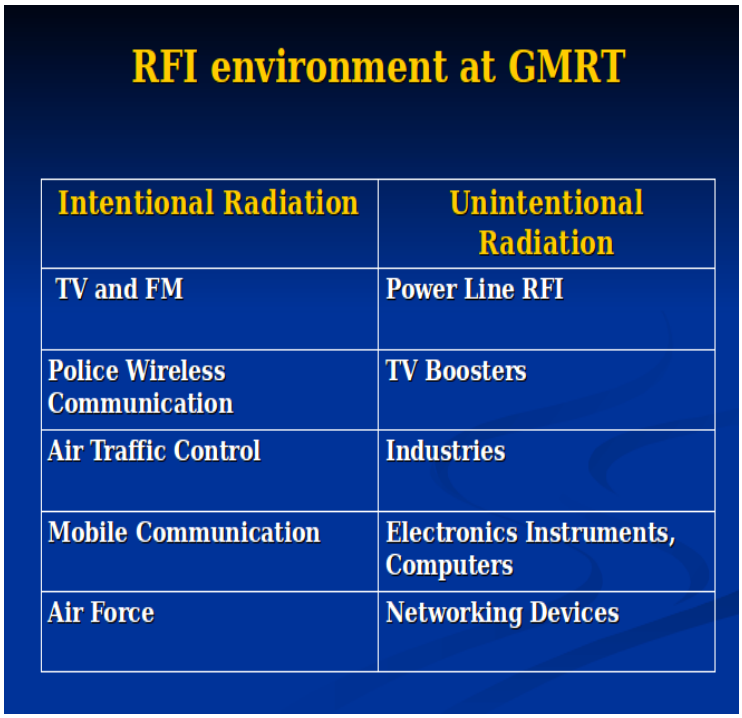

Figure 7: RFI Sources

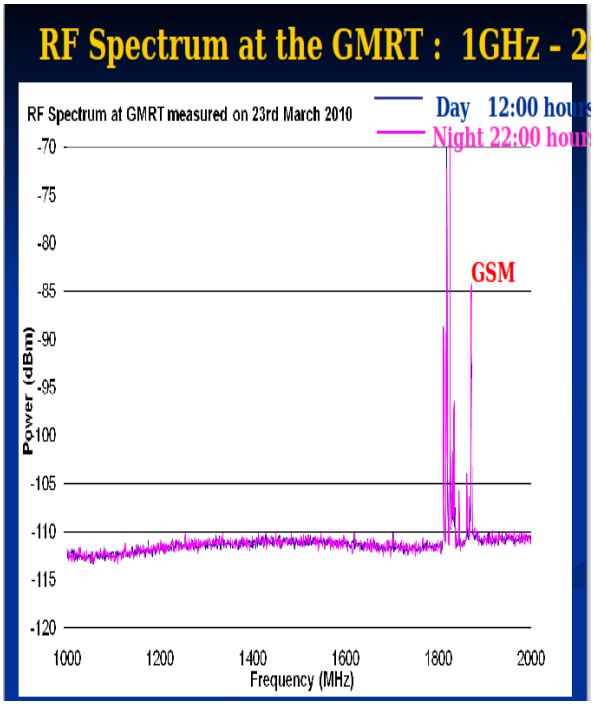

Figure 8: Radio Frequency Spectrum at GMRT

Monitoring the RFI Environment at GMRT-

- Regular Monitoring of the Radio Frequency Spectrum.
- Regular field survey to check radiation from new installations.
- Close contact and a shared knowledge base with government agencies , local industries, cellular phone operators, electric companies and individuals.
- Regular studies of internal RFI(i.e. Self-generated) , e.g. from GMRT computers, instruments.

Galaxy Cluster MASCSJ0417.5-1154 at 1.3GHz (all fields)-

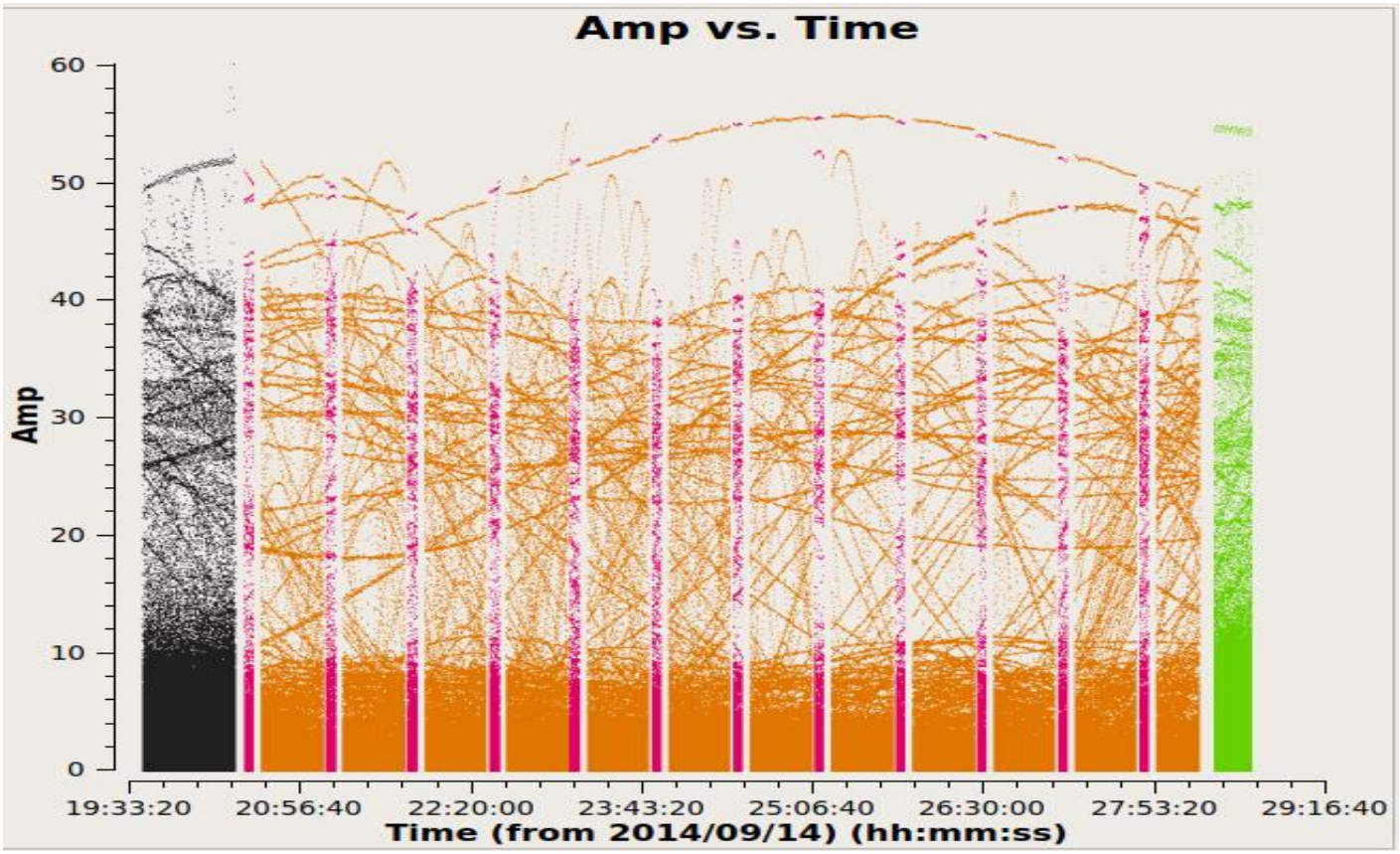

Figure 9: Amp vs. Time for all sources

- **Amplitude vs Frequency** plot of GMRT data
- Target: **MASCSJ0417.5-1154** at 1.3GHz, one of the objects studied in MAssive Cluster Survey(MACS)
- Total bandwidth of the Data is 33.33MHz.
- We can clearly see the outliers visible in our plot rendering the data of no use at this moment.
- We have to remove/flag this RFI from our data while preserving our source/calibrators data.

Removing RFI - RFI obliteration was carried out using the in-built flagdata tool in CASA. The following steps were carried out to mitigate RFI effects:-

1. Shadowed Antennas- There may be some instances where one antenna blocks, or shadows, another. Generally, observing sources at 40 degrees elevation and higher will result in less shadowing. Task flagdata can determine and flag shadowed antennas by their location and observing direction.

```
flagdata(vis='gmrt.ms', mode='shadow', tolerance=0.0, flagbackup=False) ,
    #mode='shadow': has a subparameter tolerance=0.0 that controls how many meters of
                    shadowing overlap is allowed.
```

2. Zero-Amplitude Data- In addition to shadowing, there may be times during which the correlator writes out pure zero-valued data. In order to remove this bad data, run flagdata to remove any pure zeroes:

```
flagdata(vis='gmrt.ms', mode='clip', clipzeros=True, flagbackup=False),
    #mode='clip': is used to flag all values below a given threshold. With clipzeros=True this
mode will flag exact zero values that are sometimes being produced by the VLA correlator.
```

3. Quacking- It's common for the array to settle down at the start of a scan. Quacking is used to remove data at scan boundaries, the same edit can be applied to all scans for all baselines.

```
flagdata(vis='gmrt.ms', mode='quack', quackinterval=5.0, quackmode='beg', flagbackup=False),
                    #quackmode='beg'  : Data from the start of each scan will be flagged.
```

4. Hanning-Smoothing- Strong RFI sources can give rise to the Gibbs phenomenon. This is seen by ringing, a zig-zag pattern across the channels that neighbor the strong, usually narrow, RFI. To remedy this ringing across the frequency channels, employ the hanningsmooth algorithm via the hanningsmooth2 task. Hanning-smoothing applies a triangle kernel across the pattern which diminishes the ringing, reducing the number of channels that may look bad and get flagged. This smoothing procedure will also decrease the spectral resolution by a factor of two.

```
hanningsmooth2(vis='gmrt.ms', outputvis='SNR_G55_10s-hanning.ms', datacolumn='data')
```

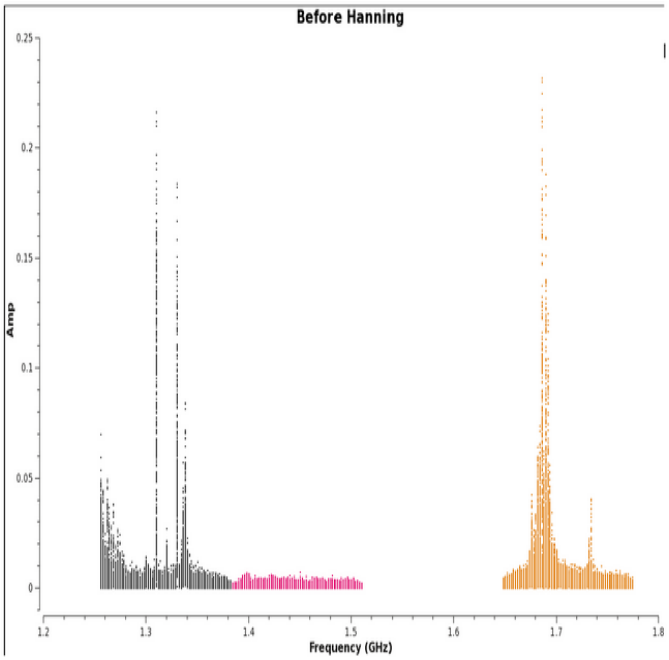

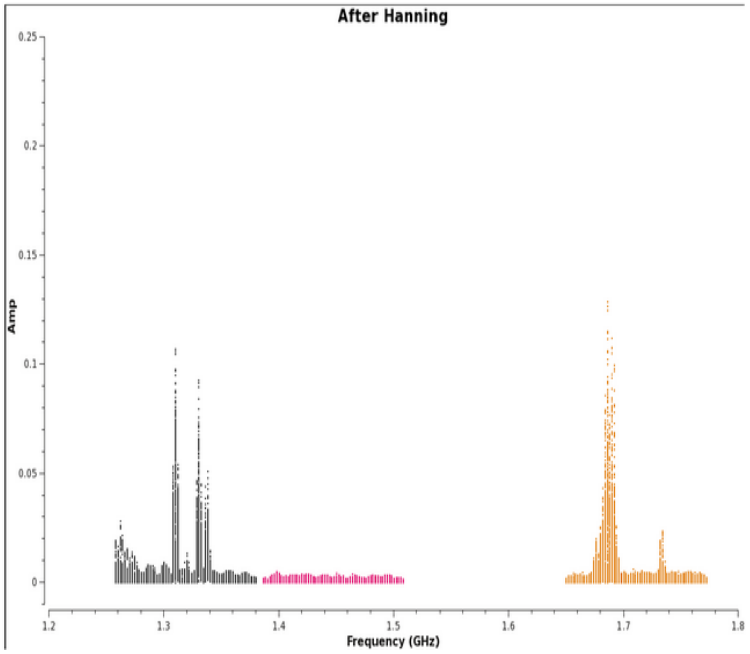

Figure10: Before Hanning Smoothing

Figure 11: After Hanning Smoothing

These plots show the effect of applying Hanning-smoothing.

5. TFCrop- Task flagdata's TFCrop is an algorithm that detects outliers in the 2D time-frequency plane and can operate on un-calibrated (non bandpass-corrected) data. TFCrop will iterate through segments of time and undergo several steps in order to find and excise different types of RFI.
Step 1: Detect short-duration RFI spikes (narrow- and broad-band).
Step 2: Search for time-persistent RFI.
Step 3: Search for time-persistent, narrow-band RFI.
Step 4: Search for low-level wings of very strong RFI.

#flagdata(vis='gmrt.ms', mode='tfcrop', spw='0', datacolumn='data', action='calculate', display='both', flagbackup=False)

Since these runs set parameters display='both' and action='calculate', the flags are displayed but not actually written to the MS. This allows one to try different sets of parameters before actually applying the flags to the data.

#flagdata(vis='gmrt.ms', mode='tfcrop', spw='0', datacolumn='data', a ction='apply', display='', flagbackup=False)

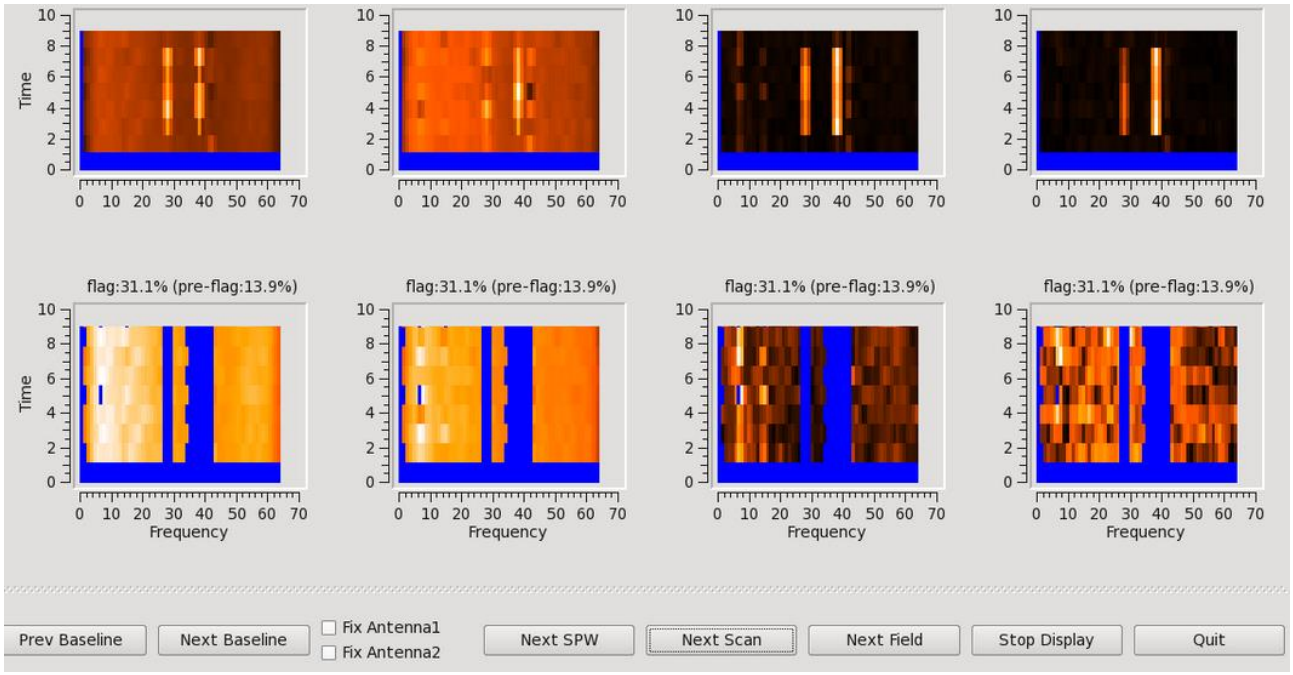

Figure12: TFCrop Flagging Results

TFCrop flagging results. Top row before, bottom row, after tfcrop.

The first row shows the data with current flags applied and the second includes the flags generated by flagdata. The x-axis is channel number (the spectral window ID is displayed in the top title) and the y-axis of the first two rows is all integrations included in a time segment.

6. Rflag- RFlag, like TFCrop, is an autoflag algorithm which uses a sliding window statistical filter. Data is iterated through in segments of time, where statistics are accumulated and thresholds calculated. In order to get the best possible result from the automatic RFI excision with flagdata's mode rflag, we will first apply bandpass calibration to the MS. Since the RFI is time-variable, using the phase calibration source to make an average bandpass over the entire observing session will mitigate the amount of RFI present in the calculated bandpass. Since there are likely to be gain variations over the course of the observing session, we will run gaincal to solve for an initial set of antenna-based phases over a narrow range of channels. Those solutions will be applied to the data when the bandpass solutions are determined. While amplitude variations will have little effect on the bandpass solutions, it is important to solve for these phase variations with sufficient time resolution to prevent decorrelation when vector averaging the data in computing the bandpass solutions. It's important to solve only for phase using a narrow channel range, since an antenna-specific delay will cause the phase to vary with respect to frequency over the spectral window, perhaps by a substantial amount.

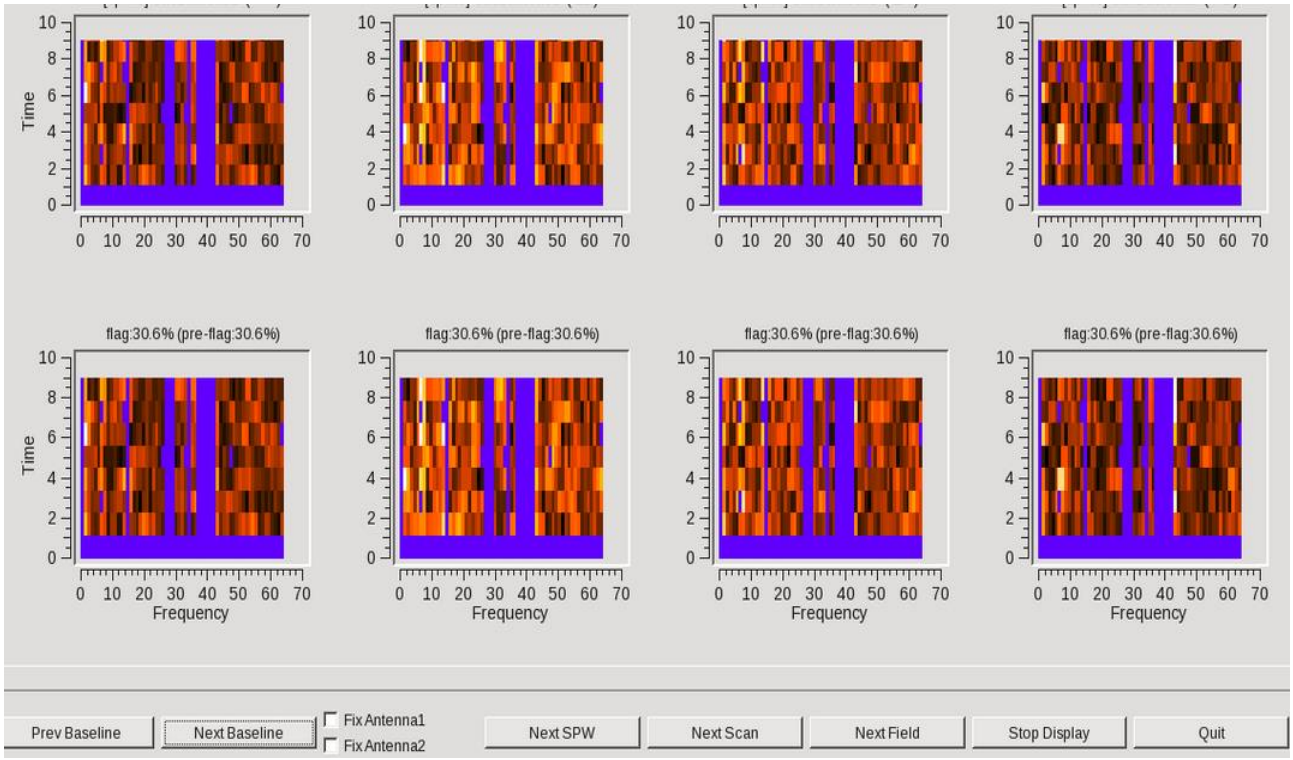

Figure 13: RFlag Results

RFlag with Default Parameters

#flagdata(vis='gmrt.ms', mode='rflag', spw='0', datacolumn='corrected', action='calculate', display='both', flagbackup=False)

Although RFlag has done a pretty good job of finding the bad data, some still remains. One way to excise the remaining bad data is to use parameter mode='extend' feature in flagdata, which can extend flags along a chosen axis and removes islands of small data patches in the midst of flagged data.

We extend the flags in time and frequency,using the parameters growtime and growfreq. We will try with parameter growtime=50.0, which will flag all data for a given channel if more than 50% of that channel's time is already flagged, and parameter growfreq=90.0, which will flag the entire spectrum for an integration if more than 90% of the channels in that integration are already flagged.

#flagdata(vis='gmrt.ms', mode='extend', spw='0', growtime=50.0, growfreq=90.0, action='apply', display='', flagbackup=False)

FINAL RESULT AFTER COMPLETING ALL STEPS-

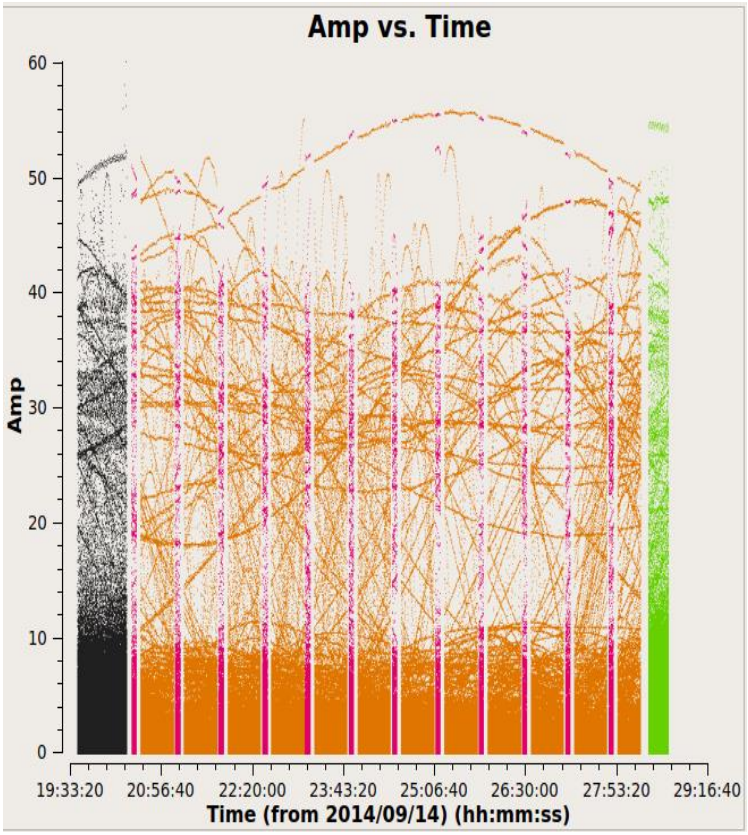

Figure 14: All Sources before RFI removal

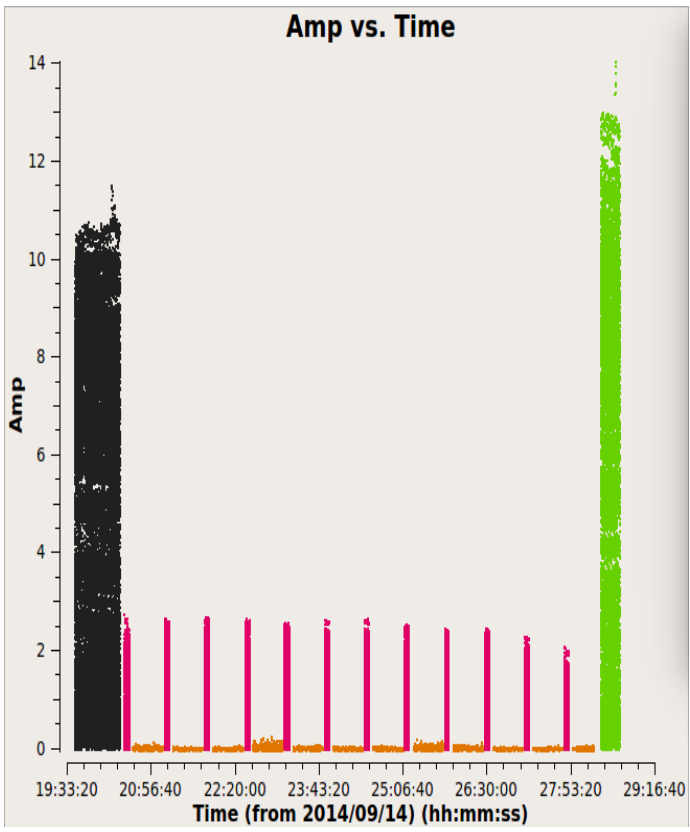

Figure 15: All Sources after RFI removal

One can clearly see the improvement in the data display after the RFI mitigation. Though some Bad data still remains, we can apply calibration processes and can minimize its effects. Now, the RFI-free uncalibrated data is ready for Calibration processes and subsequent imaging procedures.

Calibration

The main goal of calibration is to be able to correct for effects that may interfere with the scientific outcome of a measurement (an observation) due to the instrument and/or local temporary conditions so that these measurements can be compared to other measurements (at other times, other instruments, other frequencies, etc.) and theoretical predictions.

Calibration starts in the device design stage and ends in the final data presentation. Calibration can refer not only to calibration of the data, but also to the instrument as a whole or its separate components. The amount of calibration typically depends on the observing program and the science goal. Some calibrations need to be done once as their solution is fairly constant over time, while other calibrations need to be repeated regularly to capture changing properties over time. For radio astronomy, and in particular interferometry, the following general calibration steps can be identified: calibration of the instrument by observatory staff, calibration of the current observing conditions by the observer, and calibration of scientific results by the data analyzer. Some common calibration examples:

- Calibration of the antenna (receiver frequencies, receiver system temperatures, optics), antenna positions, timing, and correlator visibilities is done by observatory staff.
- Calibration of instrumental delay, instrumental polarization, spectral bandpass response, absolute flux density scale, and other possible properties—assumed to be constant during the observation—should be taken by the observer, typically once or twice during the entire observation for each observed frequency and correlator configuration.
- Calibration of antenna pointing, delay, attenuator and requantizer settings, and other possible properties assumed to be only slowly varying during the observation should be performed by the observer, typically once every hour or so during the observation, or, for example, when switching frequency bands.
- Calibration of antenna gains, atmospheric phase fluctuations, and other possible properties expected to vary more rapidly with observing conditions and geometry during the observation should be performed more frequently than the time scale over which the property changes.
- Calibration of the position of a source with respect to another source, calibration of a frequency to a line-of-sight velocity, calibration of a polarization angle to a reference angle, calibration of the flux density scale of a single source in one observation to another observation of the same source, etc.

Calibration should be performed, at the very least, more frequently than the time scale over which the property changes and before that change becomes too large to be compensated for. Nearly constant properties should be calibrated at the start of an observation, when changes from a previous observation by another observer are to be expected. If the constant property can be applied in post-processing, this calibration can also be taken at the end of the observation. Time or geometry dependent changes should be monitored at regular intervals so that the change can unambiguously be interpolated over the observation.

Typical calibration intervals are once during the observation for flux density, bandpass/delay, and polarization angle (per frequency setting and per correlator configuration). It is prudent to at least break up the flux density calibration scan into two or more separate scans, as this is the only calibration for which there is no good alternative if it happens to be corrupted. Typical intervals for complex gain (amplitude and phase) calibration are dependent on the weather conditions and baseline length. On longer baselines (i.e., on longer uv-distances and therefore more important for high frequency observing), the phase change on the interferometer will be more rapid and requires more frequent calibration than at the lower observing frequencies. An exception at low frequencies is when the Sun affects the ionosphere and rapid changes can be expected near sunset and sunrise. Otherwise, the largest effect on phase change is in the troposphere. The gain calibration uses the assumption that the calibration toward the sky, in which the calibrator source is observed, can be interpolated over time and viewing angle and resembles the same atmospheric conditions toward the sky of the target source. The further away the calibrator from the target, and the longer the intervals of the calibration measurement, the less strict this assumption will hold. It can happen that calibration consumes more than half of the allocated observing time in order to achieve the scientific goal. Fortunately, this may only be necessary at the highest frequencies, in the largest array configurations, and in bad weather conditions.

To ensure that the instrument is delivering the expected measure, the easiest method of calibration is to insert a known signal at the input and analyze the resulting signal at the output. The calibration measurement will yield, after some massaging, the corrections that need to be applied to the output signal to obtain the true representation of the input signal. A typical calibration signal for the total observational response of an interferometer is to observe a point source: a signal that can be considered a simple, single, isolated object with a known constant flux density, polarization as function of frequency, and absolute sky position. Performing a calibration on the target field—a field where obtaining the measured properties are the goal of the observation—generally is not a good idea. As a reasonable approximation in general, therefore, it is assumed that for the calibration performed near in time and near that field on the sky also holds for the target field and thus can be interpolated over the target observation.

FLUX Calibration- The correlator, where signals at specific frequencies from the antennas are combined into visibilities, only processes what it gets fed from the electronics system in terms of relative signal strength and relative phase. The correlator products, therefore, need to be readjusted to represent the flux density as measured from the sky visibilities. This means that one observes a calibrator with a postulated (or assumed) known flux density at these frequencies along with the other observations in the scheduling block. In post-processing, the visibilities are then rescaled for this calibrator to the flux density for this frequency. Other visibilities in the same observation, using the same setup, can simply be matched using the relative scale and the absolute flux density of the calibrator.

Here we bootstrapped the flux density of the calibrator by comparing the calibrator observations with observations of 3C48.CASA use model images for the standard flux density calibration sources (SETJY documentation) to account for the structures which is frequency and array configuration dependent. Alternatively, u,v restrictions, or limitations on the number of antennas, can be used.

#setjy(vis='gmrt.ms',field='3c48',standard='Perley-Butler 2013',
model='3C48_C.im',usescratch=False,scalebychan=True,spw='')
#gaincal(vis='gmrt.ms', caltable='15sepp.G0all', field='0,1,3', refant='ANT3', spw='0:113~143',
gaintype='G',calmode='p', solint='int', minsnr=5, gaintable=[''])

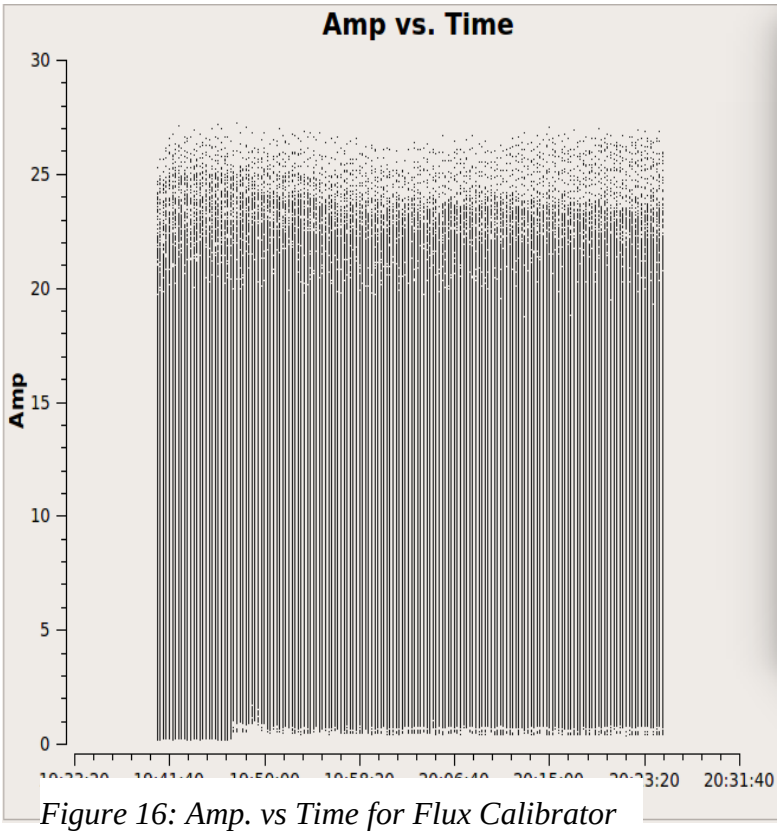

Figure 16: Amp. vs Time for Flux Calibrator 3C48

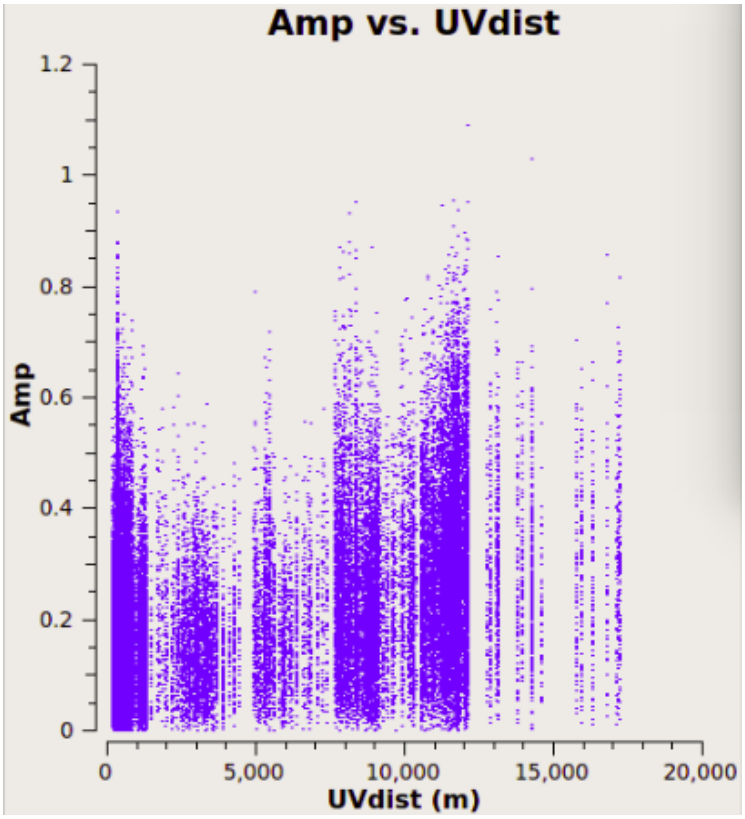

Figure 17: Amp. vs UVdist for Flux Calibrator 3C48

Bandpass and Delay Calibration-

Small impurities in the correlator model, such as an inaccurate antenna position, timing, etc., cause small deviations from the model that are noticeable as a time-constant linear phase slope as function of frequency in the correlated data. This phase slope, known as a *delay*, is a property of the IF baseband and the same for all subbands (spectral windows) in a baseband. If the frequencies in an observation are averaged into a continuum image, an uncorrected delay causes decorrelation of the continuum signal and is not a correct representation of the sky. The delay calibration is determined on a short time interval on a strong source in order to achieve high signal to noise for the solution without including the time dependent variations.

Small impurities in the frequency amplitude and phase response as function of frequency, independent of the delay, also occur and have to be corrected. These corrections are a property of the passband on top of the response of the baseband, and are a property of the subband and the location of the subband in a baseband. Leaving the *bandpass* uncorrected causes incorrect relative amplitudes and phases and does not deliver the correct spectral representation of the sky. Averaging these uncorrected impurities over frequency into a continuum image limits the achievable signal to noise and dynamic range. As for the delay, bandpass calibration is usually determined on a short time interval on a strong source to achieve high signal to noise for the solution without including the time dependent variations. Delay and bandpass calibration, therefore, is usually performed using the same calibrator. Hereafter, delay calibration is implicitly included in the bandpass calibrator or bandpass calibration scan.

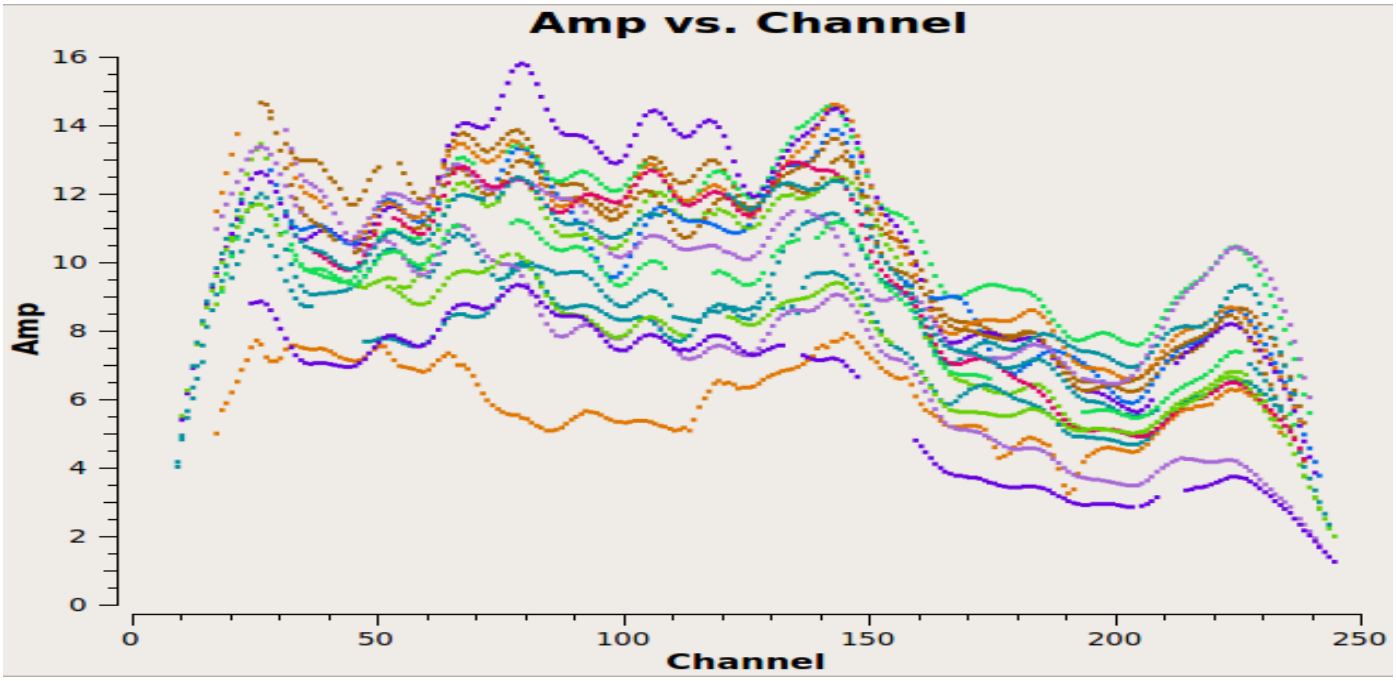

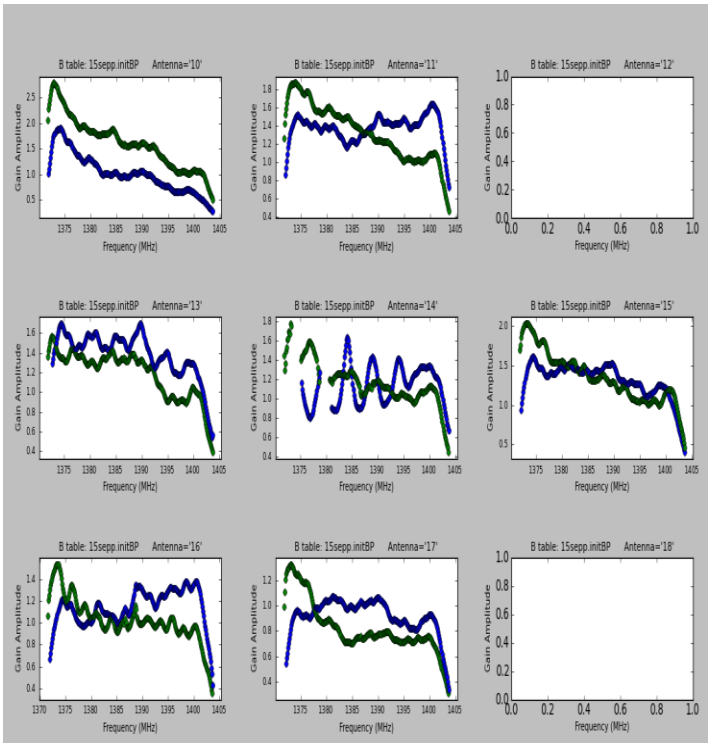

Figure 19: Gain amplitude vs frequency

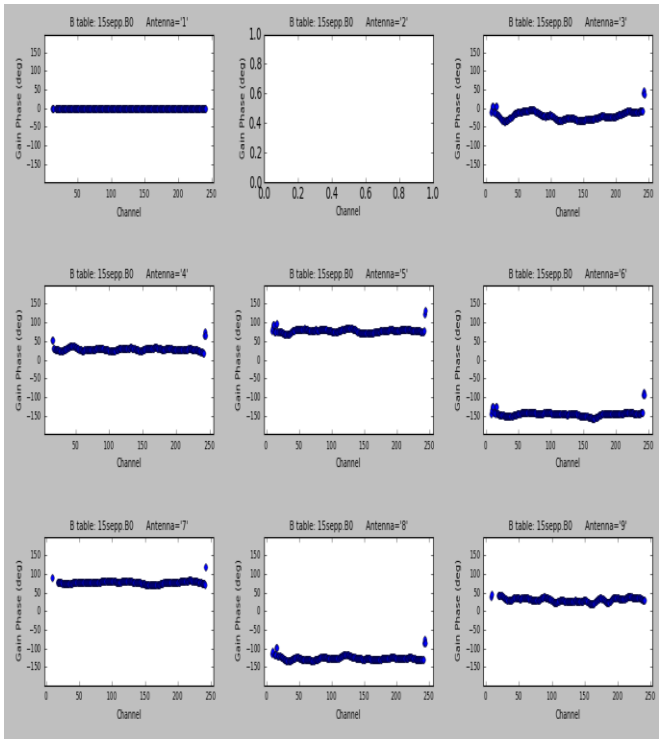

Figure 20: Gain phase vs channel

- As expected, the bandpass phases are relatively flat, with the slopes removed by the delay calibration.
- 3C48 was used as Bandpass Calibrator.

Complex Gain Calibration- Where the absolute flux density scale calibration is a static multiplier, and the bandpass/delay calibration a one-off determination of the signal path properties assumed to be largely constant for the observation, the antenna gain calibration (also known as complex gain) is anticipated to track time variable properties due to changing conditions of the instrument. Complex gain calibration also tracks changes with the environment except for antenna pointing (see below), that, if not corrected for, will be absorbed. Examples of variable instrumental properties are: receiver power level settings, corruption of baseband samplers, technicians removing receivers, etc.. The largest time variable contribution is from the environment and atmosphere: mostly the ionosphere at low frequencies, the troposphere at high frequencies, water content/opacity on cloudy days, elevation/opacity due to observing geometry and other occasional phenomena like solar flares, broadcasting satellites, tourist cell phones, digital cameras, etc. Some of these can be calibrated and corrected for using proper gain calibration while some (referred to as Radio

Frequency Interference (RFI)) cannot and need to be removed (flagged) from the data.

Gain calibration is normally considered antenna based and assumes that fluctuations in the antenna gain are due to slowly varying amplitudes and phases. Slowly here means that the interval of the gain calibration scans are short enough that the variations can be interpolated by a relative smooth function which would represent the true variation at the antenna. Gain phase varies much, much faster than gain amplitude as most of the time dependent effects affect phase more than amplitude. Additionally, phase variations scale with baseline length with more rapid changes on longer projected baselines. The typical time for such changes to become large enough to require calibration is referred to as the coherence time, i.e., when the visibility phase has changed by a radian. This coherence time may be some tens of minutes using short baselines and low frequencies or, in some realistic cases, sub-minute on long baselines for high frequency observations in non-optimal weather. Because of this huge range and frequency specific dependence, refer to the Cycle Time section at the end of this document.

#gaincal(vis='gmrt.ms',caltable='15seppp.G1', field='3c48',spw='0:10~240', solint='inf',refant='ANT3',gaintype='G',calmode='ap',solnorm=F, gaintable=['', '15sepp.K0', '15sepp.B0'], interp=['linear','linear','nearest'])

#bandtype='B' : The bandpass solution will be derived on a channel-by channel basis.

#gaintable=['', '15sepp.K0', '15sepp.B0'] : Pre-apply phase solutions, and delays.

Figure 21: Gain Phase Solutions

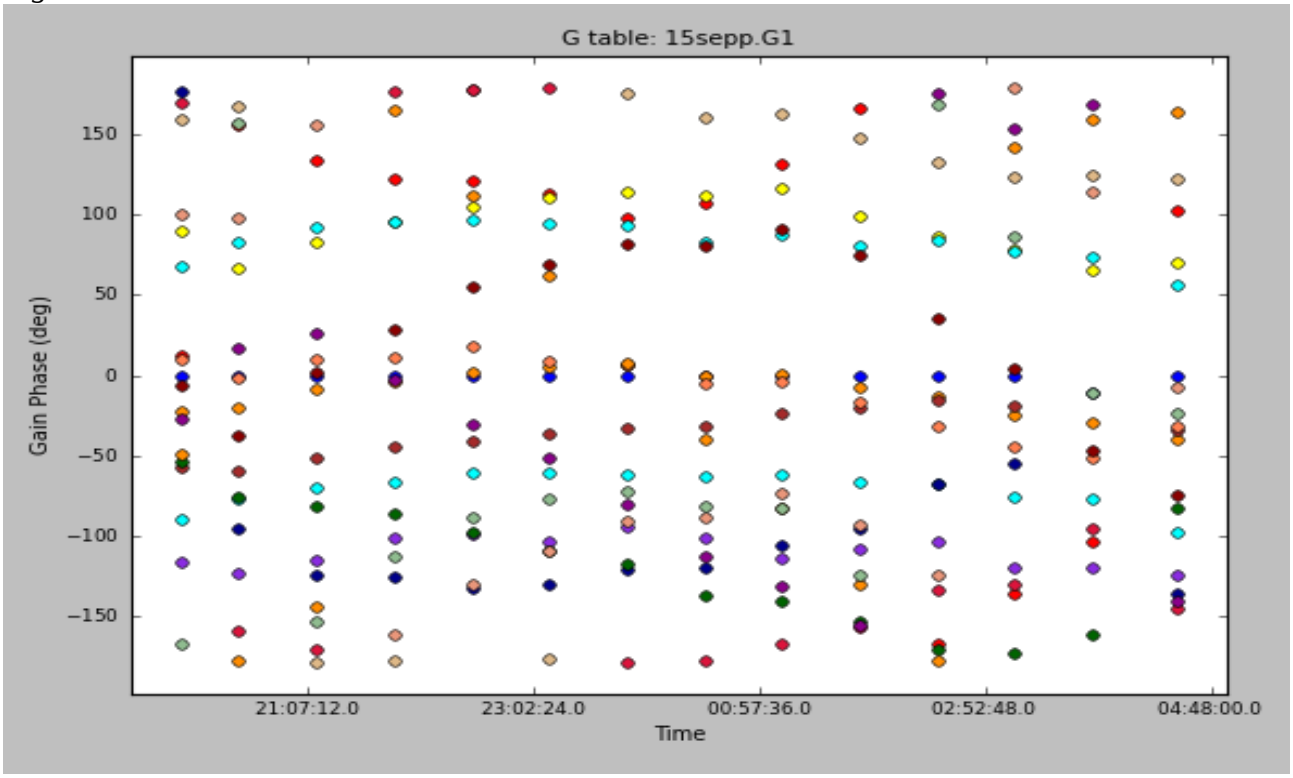

Figure 22: Gain Amplitude Solutions

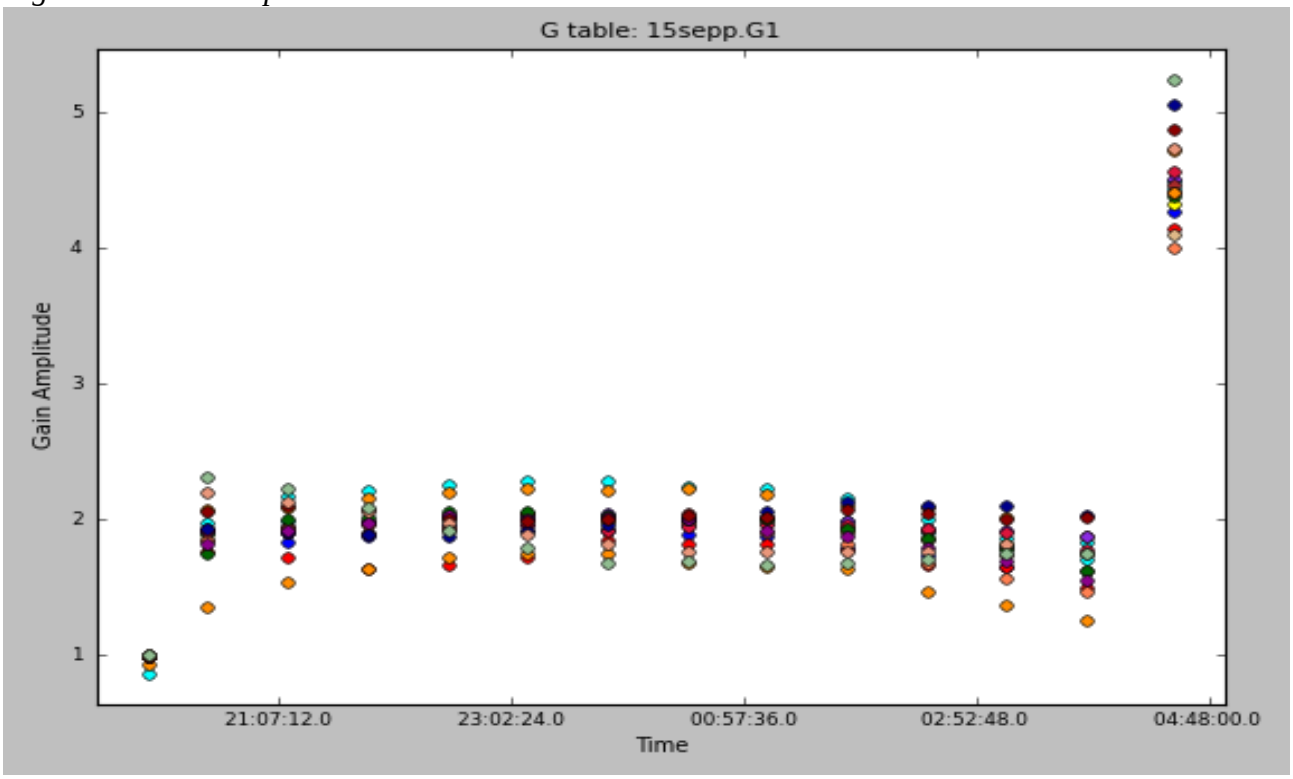

- Smooth solutions for each antenna as a function of time .

IMAGING

After performing all the necessary Calibration steps and edition we have our Calibrated Visibilities.

The following **steps are executed in order to image the data**:

1. Fit simple brightness distribution models to the visibility data.

- Works also with poorly sampled and noisy data
- Visibilities have well defined noise properties

2. Recover an image by using inverse Fourier transform:

$$I(l,m) = \mathcal{F}^{-1}\big(V(u,v)\big) \equiv \iint_{-\infty}^{\infty} V(u,v)\, e^{i2\pi(ul+vm)}\, du\, dv$$

- Complex structures can be studied
- No need to assume certain brightness distribution.

In principle, inverting $V(u,v) = \iint I(l,m)\, e^{-i2\pi(ul+vm)}\, dl\, dm$

gives the sky brightness distribution. This however requires measuring V(u,v) everywhere in the (u,v) plane. This is practically not possible. In reality, we aim to sample V(u,v) sufficiently well in order to constrain I(l,m). In any case "(u,v) coverage" is one of the main decisive factors between a high quality image and rubbish.

To do well, we want:

- Many telescopes, since the number of instantaneous (u,v) samples is N(N - 1), where N is the number of telescopes .
- Long synthesis time for changing baseline projections as Earth rotates. However, be careful if the source is variable

Formal description of a discrete sampling of the (u,v) plane-

- Visibility plane is sampled at discrete points given by sampling function:

$$S(u,v) = \sum_k \delta(u - u_k)\delta(v - v_k)$$

- If we take an inverse FT of the sampled visibility function, we get a "dirty" image:

$$I^D(l,m) = \mathcal{F}^{-1}(S(u,v)V(u,v))$$

- Convolution theorem says:

$$b(l,m) = \mathcal{F}^{-1}(S(u,v))$$

- So I(d)(l,m) a convolution of the true sky brightness distribution and the interferometer beam:

$$b(l,m) = \mathcal{F}^{-1}(S(u,v))$$

Interferometer Beam-

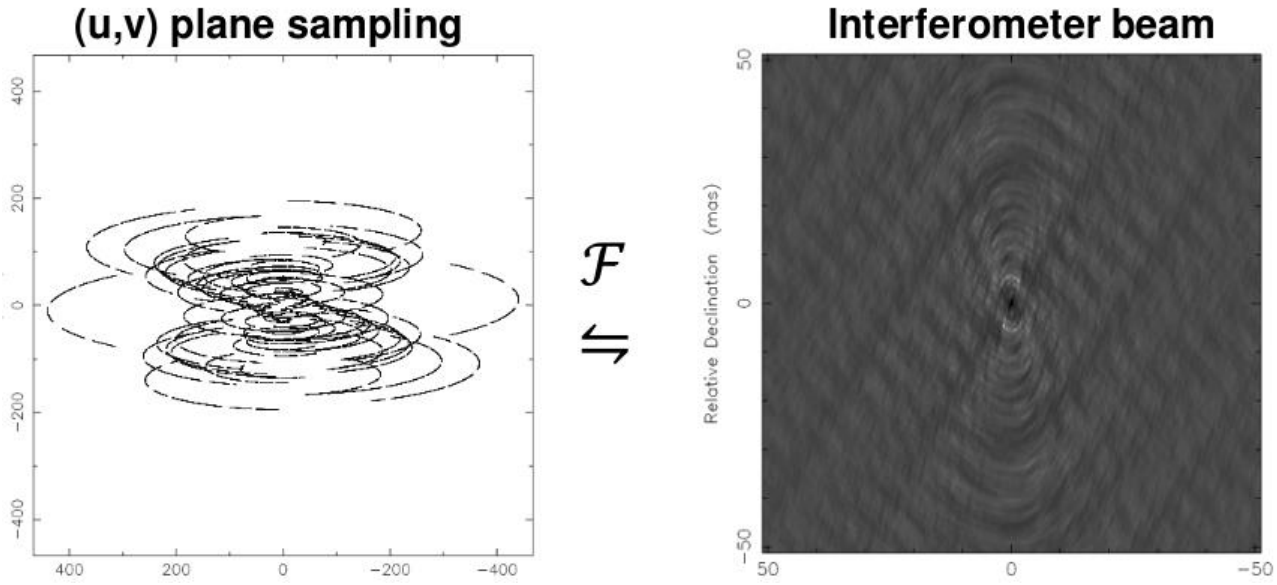

Figure 23: Interferometer beam from (u,v) sampling

Dirty Image-

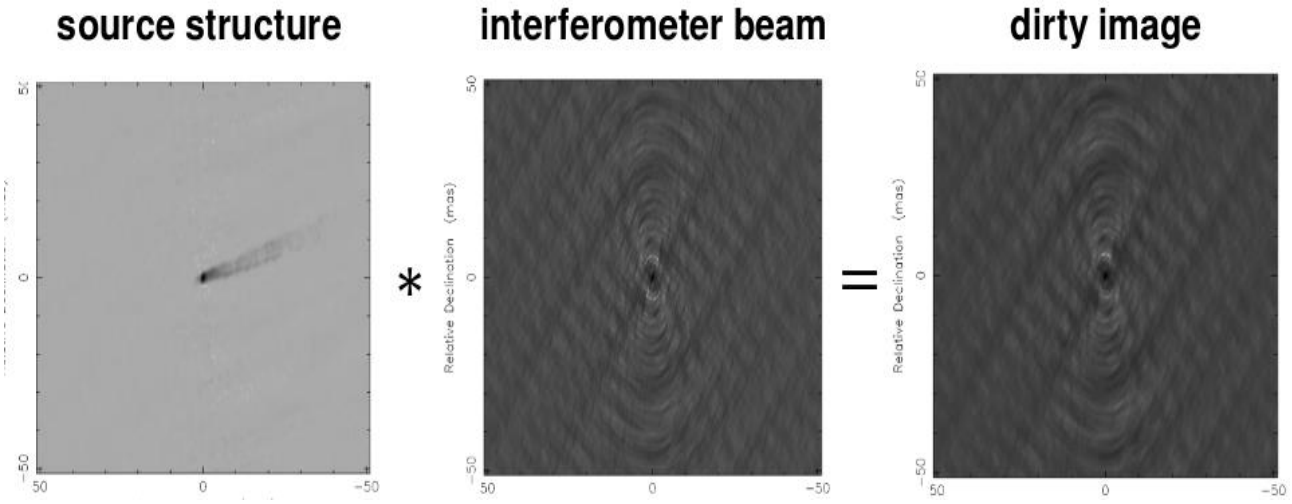

Figure 24: Dirty Image components

Practical Fourier Transformation-

- Fast Fourier Transform (FFT) is typically used to invert the data, since it is much faster than direct FT for an image of N*N pixels and N*N data points
- FFT requires data points on a rectangular grid-V(u,v) needs to be interpolated and resampled for FFT.

Image Size-

$$N\Delta l > \frac{1}{u_{min}} \text{ and } N\Delta m > \frac{1}{v_{min}}$$

Pixel Size-

Has to satisfy the Nyquist sampling theorem:

$$\Delta l \leq \frac{1}{2u_{max}} \text{ and } \Delta m \leq \frac{1}{2v_{max}}$$

Deconvolution-

Typically one uses non-linear deconvolution algorithms to interpolate and extrapolate the part of the visibility function that was not measured. These methods require some form of regularization This means that we need some a priori assumptions about the source structure in order to recover it. Luckily, quite simple assumptions suffice:

- finite source size,
- positivity of the true brightness distribution,
- Smoothness of the true brightness distribution.

Deconvolution with CLEAN algorithm-

Basic Algorithm-

Initialize: residual map = dirty map and list of δ-components = empty

- Find the peak in the residual map, identify it as a point source
- Subtract this point source, scaled by loop_gain and convolved with the interferometer beam, from the residual image
- Save the position and subtracted flux to the list of δ-components
- If stopping criteria are not met, go to initial step.
- Stop when Target noise level reached, target SNR reached, or some maximum number of iterations reached.
- Final step –make "restored" image:

1. Make a model image from the final list of δ-components
2. Convolve the model image with a "CLEAN beam", which is typically a Gaussian fitted to the central peak of the interferometer beam.
3. Add the last residual map to present the noise.

- The resulting image is an estimate of I(l,m). The units are typically Jy/ clean_beam_area.

After executing CLEAN-

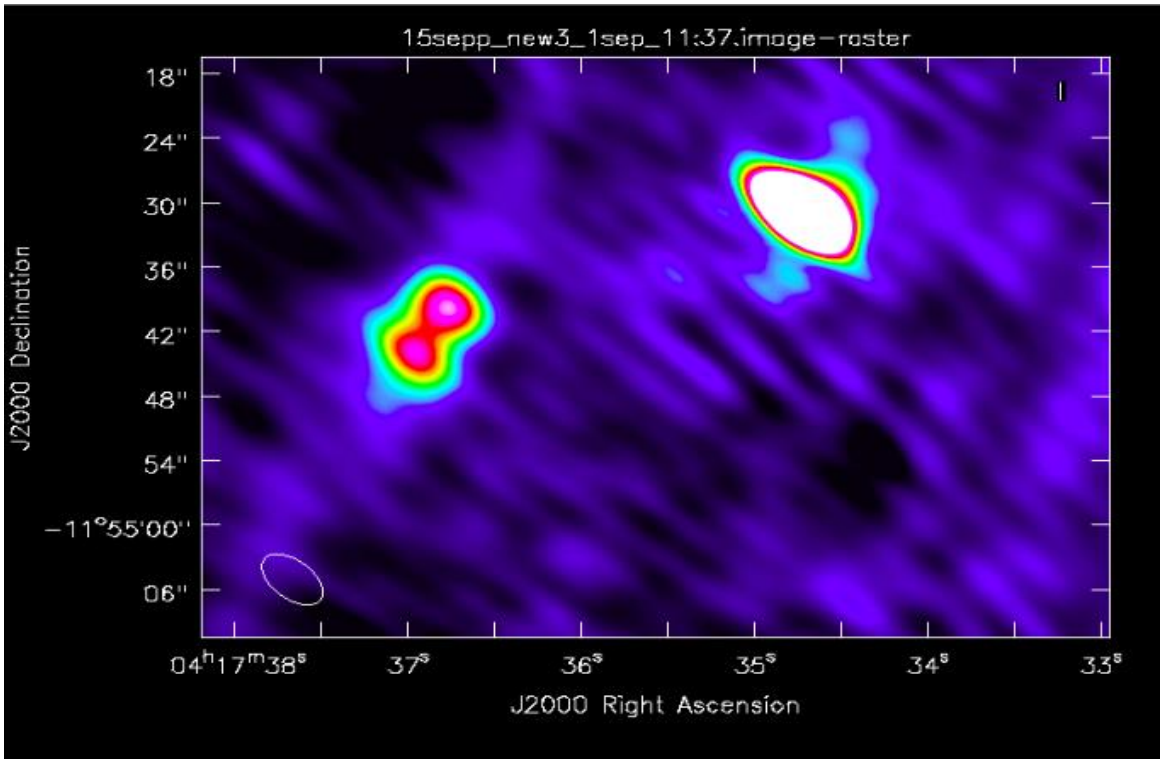

Figure 25: Initial Image without Self-Calibration

(INITIAL IMAGE WITHOUT SELF-CALIBRATION)

The blue stripes we see are the image artifacts that we wish to minimize. Bad Baselines, subtle differences in phase calibration, small atmospheric distortions which cannot be removed from calibration.To eliminate such defects, we used SELF-CALIBRATION technique.

SELF-CALIBRATION-

Even after performing all types of calibrations we encounter many subtle gains that are left in our data and disrupts the imaging process.These types of obscure gains can be tackled to some extent by applying Self-Calibration technique. STEPS involving Self-Calibration:

1. Make an initial model of the source using constraints on the source structure.
2. Use this model to solve for the gains
3. Find the corrected visibility
4. Form a new model using this corrected data
5. Repeat step 2.

Improvement in Image after 1 round of self-calibration:

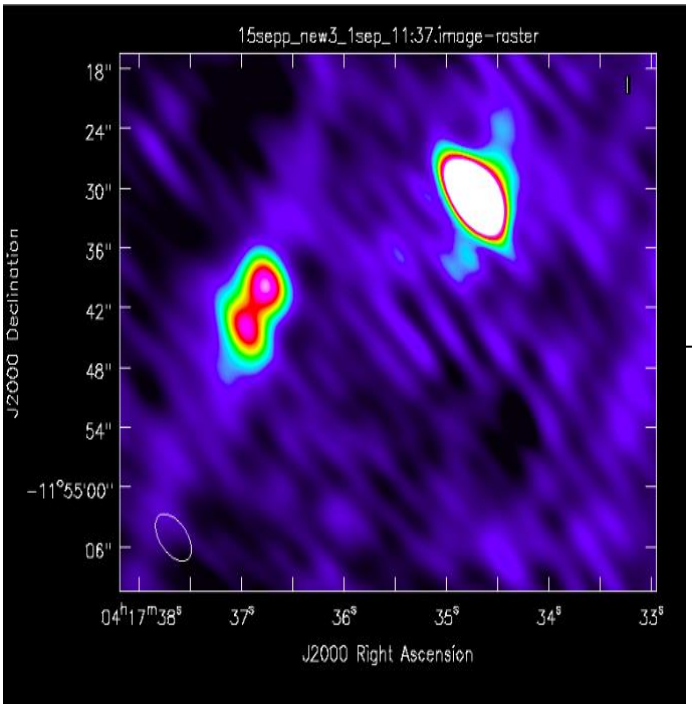

Figure 26: Initial Image without Self-Calibration

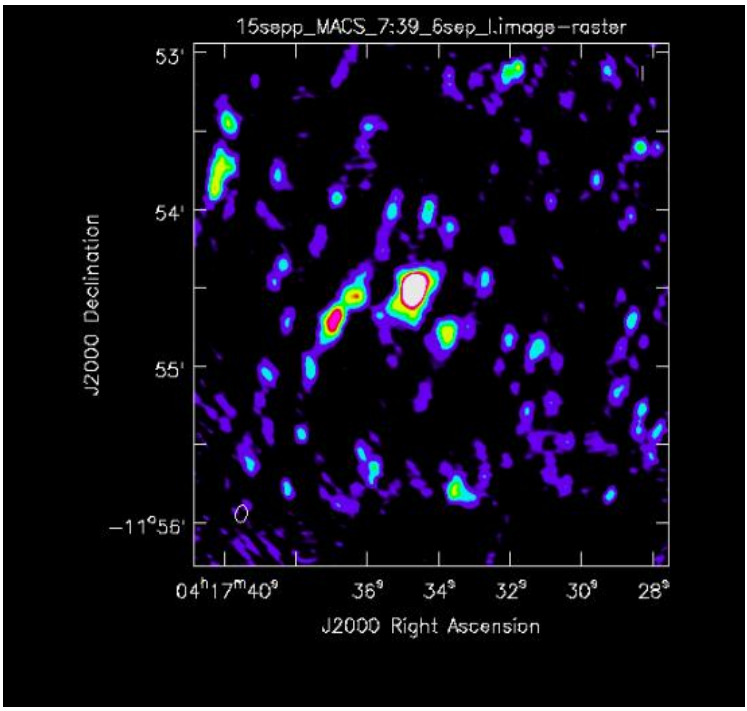

Figure 27: Image after a round of Self-Calibration

Repeated iterations of Self-Calibration is performed to obtain image improvements.The stripes are begining to fade off and we are able to see much clearer image in which we can identify emissions.

FINAL IMAGE-

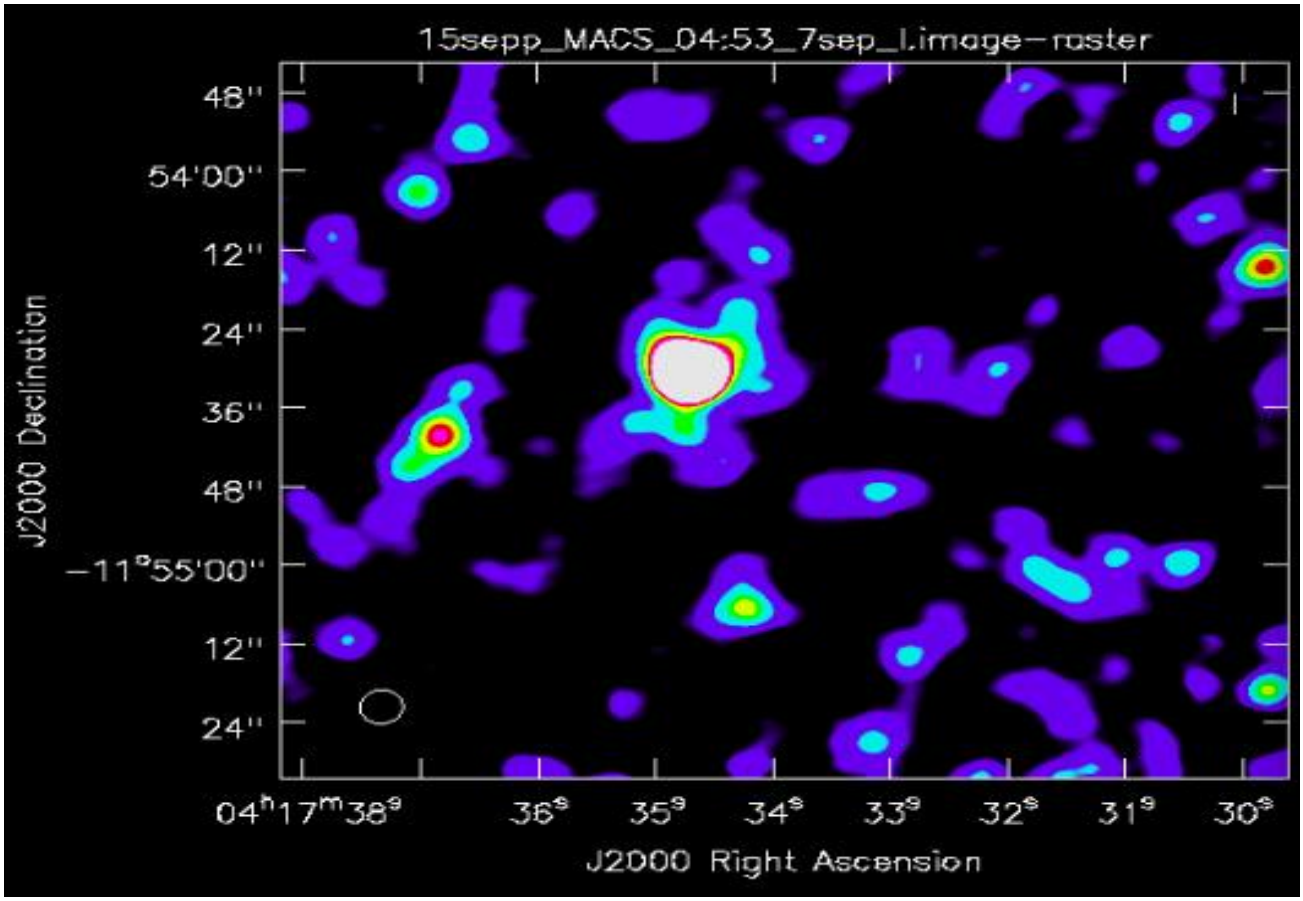

Figure 28: Final Image after 3 rounds of Self-calibration

After performing three rounds of Self-Calibration.

- Dynamic Range of over 100 is observed.
- Image artifacts are reduced to a minimum, after performing multiple iterations.
- Diffuse emissions can be seen on multiple spots.
- Simulations can be performed on this image to gain further information.

Conclusion and Future Scope-

Diffuse Radio emissions are detected on multiple spots in cluster **MASCSJ0417.5-1154.** Whether it's a Radio halo or some other source of emission is up to further exploration. Galaxy Clusters are unique astrophysical laboratories in which the powerful interaction of supermassive black holes with the surrounding intra-cluster medium, the complex effects of the cluster environment on galaxies, as well as a wide range of non-thermal processes like magnetic field amplification and cosmic ray acceleration can be studied.

A better knowledge of the physics of the non-thermal component in galaxy clusters will have important cosmological implications. If it will be confirmed that the presence of giant halos and relics is related to cluster mergers, the statistical properties of these radio sources will allow us to test the current cluster formation scenario, giving important hints on large-scale structure formation and, thus, cosmological parameters. Additionally, we will be able to estimate how the gravitational energy released during cluster mergers is redistributed between the thermal ICM and the relativistic plasma. Further the knowledge of extended radio sources in clusters is indeed essential for complementary cosmological studies, e.g. the epoch of re-ionisation (EoR).

References:

1. **Venturi, T., Giacintucci, S., Dallacasa, D., Cassano, R., Brunetti, G., Bardelli, S., Setti, G.2008, Astron. Astrophys., 484, 327.**
2. **Ebeling, H., Edge, A. C., Mantz, A., Barrett, E., Henry, J. Patrick, Ma, C. J., van Speybroeck,L. 2010, Mon. Not. R. Astron. Soc., 407, 83.**
3. **Van Speybroeck,L. 2010, Mon. Not. R. Astron. Soc., 407, 83. Dolag & Schindler 2000, Dolag et al. 2001a, Colafrancesco et al. 2004**
4. **Di Matteo et al. 2004; The clustering of active galactic nuclei in the Sloan Digital Sky Survey ;**
5. **The National Radio Astronomy Observatory (http://www.nrao.edu/)**
6. **K. S. Dwarakanath, Siddharth Malu & Ruta Kale : Discovery of a Giant Radio Halo in a Massive Merging Cluster**
7. **CASA guides(casaguides**.nrao.edu**)**
8. **S.T. Myers et al : Galaxy Cluster Astrophysics and Cosmology: Questions and Opportunities for the Coming Decade**
9. **Luigina Feretti, Gabriele Giovannini, Federica Govoni, Matteo Murgia: Clusters of galaxies- observational properties of the diffuse radio emission**